

# Astrophysical reaction rate for ${}^9\text{Be}$ formation within a three-body approach

J. Casal,\* M. Rodríguez-Gallardo, and J. M. Arias

*Departamento de Física Atómica, Molecular y Nuclear, Facultad de Física, Universidad de Sevilla, Apartado 1065, E-41080 Sevilla, Spain*

I. J. Thompson

*Lawrence Livermore National Laboratory, L-414, Livermore, California 94551, USA*

(Received 23 July 2014; revised manuscript received 9 September 2014; published 6 October 2014; corrected 16 December 2016)

The structure of the Borromean nucleus  ${}^9\text{Be}$  ( $\alpha + \alpha + n$ ) is addressed within a three-body approach using the analytical transformed harmonic oscillator method. The three-body formalism provides an accurate description of the radiative capture reaction rate for the entire temperature range relevant in astrophysics. At high temperatures, results match the calculations based on two-step sequential processes. At low temperatures, where the particles have no access to intermediate two-body resonances, the three-body direct capture leads to reaction rates larger than the sequential processes. These results support the reliability of the method for systems with several charged particles.

DOI: [10.1103/PhysRevC.90.044304](https://doi.org/10.1103/PhysRevC.90.044304)

PACS number(s): 21.45.-v, 26.20.-f, 26.30.-k, 27.20.+n

## I. INTRODUCTION

The origin of elements in the Universe is an important topic in nuclear astrophysics [1]. The formation of heavy nuclei from light elements needs to overcome the instability gaps at mass numbers  $A = 5$  and  $A = 8$  [2]. At the helium burning stage of stars, the triple- $\alpha$  reaction for the formation of  ${}^{12}\text{C}$  is the main nucleosynthesis process. However, in neutron rich environments, the reaction  $\alpha(\alpha n, \gamma){}^9\text{Be}$  followed by  ${}^9\text{Be}(\alpha, n){}^{12}\text{C}$  may dominate, depending on the astrophysical conditions [3]. The relevance of this process has been linked to the nucleosynthesis by rapid neutron capture (or  $r$  process) in type II supernovae [3–6], so establishing an accurate rate for the formation of  ${}^9\text{Be}$  is essential for the  $r$ -process abundance predictions [7,8].

The radiative three-body capture processes are essential in overcoming the  $A = 5, 8$  gaps [2,9], but traditionally they have been described as two-step sequential reactions [1,3,10–13]. When at least one of the two-body subsystems shows a low-lying narrow resonance, the sequential picture provides a rather accurate description of these reactions for high-temperature environments, where the intermediate states can be populated. However, at low temperatures the particles may have no energy to populate intermediate resonances, and therefore the direct three-body capture plays an important role [14–16]. Moreover, the intermediate configurations may not be present or show a too quick decay. So, a complete three-body formulation is needed to describe properly the reaction rates of such nuclei in the entire temperature range.

The complete computation of three-body reactions in the whole energy range requires a narrow grid of continuum states right above the breakup threshold [14], which is a difficult task. The asymptotic behavior of continuum states for systems with several charged particles is not known in general, and very involved procedures are needed to deal with this problem [16–18]. In a recent work [19,20] we presented a pseudostate (PS) method based on an analytical local

scale transformation (LST) of the harmonic oscillator (HO) basis, the transformed harmonic oscillator (THO) method. We generalized the analytical THO method for three-body systems and successfully applied it to the Borromean nucleus  ${}^6\text{He}$  ( $\alpha + n + n$ ) system. PS methods consist of diagonalizing the Hamiltonian in a complete set of square-integrable functions, a procedure which does not require going through the continuum wave functions, and the previous knowledge of the asymptotic behavior is not needed. Furthermore, in the analytical THO method, the parameters of the transformation govern the radial extension of the THO basis. This provides the advantage of allowing the construction of an optimal basis for each observable of interest [19,21,22]. The analytical THO basis can describe very accurately the strength functions in the low-energy range, providing a good description of the radiative capture reactions.

In the present work we apply the analytical THO method to the Borromean nucleus  ${}^9\text{Be}$ , whose astrophysical relevance has been pointed out. The purpose of this paper is to show the reliability of the method when applied to systems with more than one charged particle, and to confirm the importance of the direct three-body capture at low temperature. The full three-body formalism allows the treatment of the direct and sequential, resonant and nonresonant processes on the same footing. Thus these processes do not need to be treated separately when estimating the total contribution to the astrophysical reaction rate [16,23].

The paper is structured as follows. In Sec. II the three-body formalism is presented. The analytical THO method and the expression for the radiative capture reaction rate are shown. The electromagnetic transition probabilities are derived for a system with two identical charged particles. In Sec. III the full formalism is applied to the case of  ${}^9\text{Be}$ , and the rate of the radiative capture reaction  $\alpha + \alpha + n \rightarrow {}^9\text{Be} + \gamma$  is obtained. Finally, in Sec. IV, the main conclusions of this work are summarized.

## II. THREE-BODY FORMALISM

The three-body formalism used in this work is described in detail in Ref. [19], where it is applied to a system with a

\*jcasal@us.es

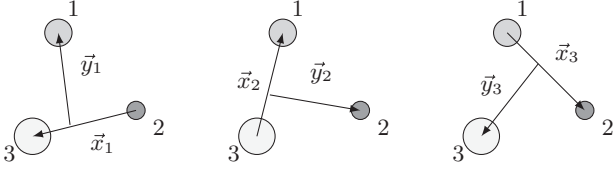


FIG. 1. The three sets of scaled Jacobi coordinates.

single charged particle. In this section, we summarize the main features of the formalism and we derive the electromagnetic transition probabilities  $B(\mathcal{O}\lambda)$  for the case of a system with two identical charged particles, such as  ${}^9\text{Be}$  ( $\alpha + \alpha + n$ ).

In order to describe the three-body system we use hyperspherical coordinates  $\{\rho, \alpha_k, \hat{x}_k, \hat{y}_k\}$ , which are obtained from the Jacobi coordinates  $\{\mathbf{x}_k, \mathbf{y}_k\}$ . Note that there are three possible Jacobi systems, each one denoted by the label  $k = 1, 2, 3$ . The variable  $\mathbf{x}_k$  is proportional to the relative coordinate between two of the particles and  $\mathbf{y}_k$  is proportional to the coordinate from the center of mass of these two particles to the third one, both with a scaling factor depending on their masses [24]. We are using the odd-man-out notation in which, for example, the Jacobi-1 system corresponds to the Jacobi system in which the particles (2,3) are related by the coordinate  $\mathbf{x}_1$  (see Fig. 1).

The hyperradius  $\rho$  and the hyperangle  $\alpha_k$  are related to the Jacobi coordinates as

$$\rho = \sqrt{x_k^2 + y_k^2}, \quad (1)$$

$$\alpha_k = \tan\left(\frac{x_k}{y_k}\right). \quad (2)$$

While the hyperangle depends on the Jacobi- $k$  system, the hyperradius does not.

### A. Analytical THO

The THO method consists of diagonalizing the Hamiltonian of the system in a discrete basis of  $\mathcal{L}^2$  functions, the THO functions, in one of the Jacobi systems (for simplicity, if  $k$  is fixed we do not specify it)

$$\psi_{i\beta j\mu}^{\text{THO}}(\rho, \Omega) = R_{i\beta}^{\text{THO}}(\rho) \mathcal{Y}_{\beta j\mu}(\Omega), \quad (3)$$

where  $\Omega \equiv \{\alpha, \hat{x}, \hat{y}\}$  is introduced for the angular dependence and  $\beta \equiv \{K, l_x, l_y, l, S_x, j_{ab}\}$  is a set of quantum numbers called a channel. In this set,  $K$  is the hypermomentum,  $l_x$  and  $l_y$  are the orbital angular momenta associated with the Jacobi coordinates  $\mathbf{x}$  and  $\mathbf{y}$ , respectively,  $l$  is the total orbital angular momentum ( $l = l_x + l_y$ ),  $S_x$  is the spin of the particles related by the coordinate  $\mathbf{x}$ , and  $j_{ab}$  results from the coupling  $\mathbf{j}_{ab} = l + S_x$ . If we denote by  $I$  the spin of the third particle, that we assume to be fixed, the total angular momentum  $j$  is  $j = j_{ab} + I$ . The functions  $\mathcal{Y}_{\beta j\mu}(\Omega)$  are states of good total angular momentum, expanded in hyperspherical harmonics (HH) [25,26] as shown in Appendix A [see Eq. (A2)].

The THO hyperradial functions  $R_{i\beta}^{\text{THO}}(\rho)$  are based on a LST,  $s(\rho)$ , of the HO functions:

$$R_{i\beta}^{\text{THO}}(\rho) = \sqrt{\frac{ds}{d\rho}} R_{iK}^{\text{HO}}[s(\rho)], \quad (4)$$

where  $i$  denotes the hyperradial excitation. In this paper, as in Refs. [19,21,22], we adopt the analytical form of Karataglidis *et al.* [27],

$$s(\rho) = \frac{1}{\sqrt{2b}} \left[ \frac{1}{\left(\frac{1}{\rho}\right)^\xi + \left(\frac{1}{\gamma\sqrt{\rho}}\right)^\xi} \right]^{\frac{1}{\sigma}}, \quad (5)$$

depending on the parameters  $\xi$ ,  $\gamma$ , and the oscillator length  $b$ . The HO hyperradial variable  $s$  is dimensionless according to the transformation defined above [Eq. (5)]. In this way, we take the oscillator length  $b$  as another parameter of the transformation. We have fixed for all calculations  $\xi = 4$  as in Ref. [19], since a very weak dependence of the results on this parameter was found previously. Note that the THO hyperradial wave functions depend, in general, on all the quantum numbers included in a channel  $\beta$ , however the HO hyperradial wave functions only depend on the hypermomentum  $K$ .

The states of the system are then given by diagonalization of the three-body Hamiltonian in a finite basis up to a maximum hypermomentum  $K_{\text{max}}$ , which determines the number of channels, and  $i_{\text{max}}$  hyperradial excitations in each channel,

$$\Psi_{n j\mu}(\rho, \Omega) = \sum_{\beta} \sum_{i=0}^{i_{\text{max}}} C_n^{i\beta j} R_{i\beta}^{\text{THO}}(\rho) \mathcal{Y}_{\beta j\mu}(\Omega), \quad (6)$$

where  $C_n^{i\beta j}$  are the diagonalization coefficients, and the label  $n$  enumerates the eigenstates.

The function  $s(\rho)$  behaves asymptotically as  $\frac{\gamma}{b} \sqrt{\frac{\rho}{2}}$  and hence the THO hyperradial wave functions obtained behave at large distances as  $\exp(-\gamma^2 \rho / 2b^2)$ . Therefore, the ratio  $\gamma/b$  governs the asymptotic behavior of the THO functions: as  $\gamma/b$  increases, the hyperradial extension of the basis decreases and some of the eigenvalues obtained by diagonalizing the Hamiltonian explore higher energies [21]. That is,  $\gamma/b$  determines the density of PSs as a function of the energy. This gives the freedom to choose an appropriate basis depending on the observable of interest.

### B. Radiative capture reaction rate

We consider the radiative capture reaction of three particles,  $(abc)$ , into a bound nucleus  $A$  of binding energy  $|\varepsilon_B|$ , i.e.,  $a + b + c \rightarrow A + \gamma$ . The energy-averaged reaction rate for such process,  $\langle R_{abc}(\varepsilon) \rangle$ , is given as a function of the temperature  $T$  by the expression [14,19]

$$\langle R_{abc}(\varepsilon) \rangle(T) = v! \frac{\hbar^3}{c^2} \frac{8\pi}{(a_x a_y)^{3/2}} \frac{g_A}{g_a g_b g_c} \frac{1}{(k_B T)^3} \times \int_0^\infty (\varepsilon + |\varepsilon_B|)^2 \sigma_\gamma(\varepsilon + |\varepsilon_B|) e^{-\frac{\varepsilon}{k_B T}} d\varepsilon. \quad (7)$$

where  $\varepsilon = \varepsilon_\gamma + \varepsilon_B$  is the initial three-body kinetic energy,  $\varepsilon_\gamma$  is the energy of the photon emitted,  $\varepsilon_B$  is the ground-state

energy,  $g_i$  are the spin degeneracies of the particles,  $\nu$  is the number of identical particles in the three-body system,  $a_x$  and  $a_y$  are the reduced masses of the subsystems related to the Jacobi coordinates  $\{\mathbf{x}, \mathbf{y}\}$ , and  $\sigma_\gamma(\varepsilon_\gamma)$  is the photodissociation cross section of the system  $A$ . This function can be expanded into electric and magnetic multipoles [15,28],

$$\sigma_\gamma^{(\mathcal{O}\lambda)}(\varepsilon_\gamma) = \frac{(2\pi)^3(\lambda+1)}{\lambda[(2\lambda+1)!!]^2} \left(\frac{\varepsilon_\gamma}{\hbar c}\right)^{2\lambda-1} \frac{dB(\mathcal{O}\lambda)}{d\varepsilon}, \quad (8)$$

which are related to the transition probability distributions  $dB(\mathcal{O}\lambda)/d\varepsilon$ , for  $\mathcal{O} = E, M$ .

The integral in Eq. (7) is very sensitive to the  $dB(\mathcal{O}\lambda)/d\varepsilon$  behavior at low energy and, for that reason, a detailed description of the transition probability distribution in that region is needed to avoid numerical errors. Accordingly to the traditional literature [29], in the absence of low-energy resonances the first multipole contribution is the dominant one and the electric contribution dominates over the magnetic one at the same order.

### C. Electromagnetic transition probability $B(\mathcal{O}\lambda)$

As in Refs. [19,24], we follow the notation of Brink and Satchler [30]. The reduced transition probability between states of the system is defined as

$$\begin{aligned} B(\mathcal{O}\lambda)_{n_j, n' j'} &\equiv B(\mathcal{O}\lambda; n_j \rightarrow n' j') \\ &= |\langle n_j || \widehat{\mathcal{O}}_\lambda || n' j' \rangle|^2 \left(\frac{2\lambda+1}{4\pi}\right), \end{aligned} \quad (9)$$

where  $\widehat{\mathcal{O}}_{\lambda M_\lambda}$  is the electric or magnetic multipole operator of order  $\lambda$ , and the  $|n_j \mu\rangle$  denotes the wave function given by Eq. (6).

We consider first electric transitions, involving the matrix elements of the electric multipole operator  $\widehat{Q}_{\lambda M_\lambda}$ . This operator, for a general system with three particles, takes the form in the Jacobi- $k$  set

$$\widehat{Q}_{\lambda M_\lambda}(\mathbf{x}_k, \mathbf{y}_k) = \left(\frac{4\pi}{2\lambda+1}\right)^{1/2} \sum_{q=1}^3 Z_q e r_q^\lambda Y_{\lambda M_\lambda}(\widehat{r}_q), \quad (10)$$

where  $Z_q$  is the atomic number of the particle  $q$ ,  $e$  is the electron charge, and  $\mathbf{r}_q$  is the position of particle  $q$  with respect to the center of mass of the system, which in the Jacobi- $q$  system is given by [31]

$$\mathbf{r}_q = \sqrt{\frac{m}{m_q} \frac{(M_T - m_q)}{M_T}} \mathbf{y}_q. \quad (11)$$

Here  $m$  is a normalization mass, taken as the atomic mass unit, and  $M_T$  is the total mass of the system. We describe the system in a preferred Jacobi set,  $k$ , however the expression for the electric multipole operator given by Eq. (9) can be easily expressed, in general, using different Jacobi systems. The relation between harmonic polynomials in different Jacobi

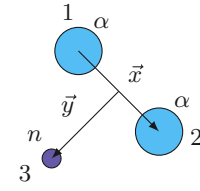


FIG. 2. (Color online)  ${}^9\text{Be}$  in Jacobi- $T$  system.

sets is given by the expression [32]

$$\begin{aligned} y_q^\lambda Y_{\lambda M_\lambda}(\widehat{y}_q) &= \sum_{l=0}^{\lambda} (-1)^l x_k^{\lambda-l} (\sin \varphi_{qk})^{\lambda-l} y_k^l (\cos \varphi_{qk})^l \\ &\times \sqrt{\frac{4\pi(2\lambda+1)!}{(2l+1)!(2\lambda-2l+1)!}} \\ &\times [Y_{\lambda-l}(\widehat{x}_k) \otimes Y_l(\widehat{y}_k)]^{\lambda M_\lambda}, \end{aligned} \quad (12)$$

with

$$\tan \varphi_{qk} = (-1)^P \sqrt{\frac{m_p M_T}{m_q m_k}}, \quad (13)$$

depending on the mass of the particles and the parity  $(-1)^P$  of the permutation  $P$  of  $\{k, p, q\}$ . The identity transformation is given by  $\varphi_{kk} = \pi$ . Using Eq. (12) we can rewrite the harmonic polynomial for each particle  $q$  as a function of the Jacobi coordinates in the preferred Jacobi system  $k$ . This is equivalent to rotating the functions to the Jacobi system  $q$  where the position of each particle is given by a vector proportional to  $\mathbf{y}_q$ .

If we consider a system with two identical charged particles, such as  ${}^9\text{Be}$ , we describe the problem using the Jacobi- $T$  system shown in Fig. 2. In the  $T$  system the two  $\alpha$  particles are related by the  $\mathbf{x}$  coordinate. For simplicity, the subindexes corresponding to the chosen Jacobi set are normally omitted. So in this case,  $\mathbf{x} = \mathbf{x}_3$  and  $\mathbf{y} = \mathbf{y}_3$ .

From Eqs. (11)–(13), the expression (10) can be reformulated for dipolar transitions ( $\lambda = 1$ ) as

$$\widehat{Q}_{1M_1} = -\left(\frac{4\pi}{3}\right)^{1/2} 2(\cos \varphi_{23}) Z_2 e \frac{\sqrt{m a_{y2}}}{m_2} y Y_{1M_1}(\widehat{y}). \quad (14)$$

Here  $a_{y2} = a_{y1}$  is the Jacobi mass factor related to the coordinate  $\mathbf{y}_2$ ,

$$a_{y2} = \frac{m_2(m_3 + m_1)}{M_T}, \quad (15)$$

and  $m_2 = m_1$ , in this case, is the  $\alpha$  particle mass. The  $\mathbf{x}$  component is absent in Eq. (14) because the two charged particles are identical, which simplifies the problem. This expression is analogous to Eq. (18) in Ref. [19] but including a factor  $2 \cos(\varphi_{23})$  which, for  ${}^9\text{Be}$ , equals  $2/\sqrt{10}$ .

To test the completeness of the basis, we can also calculate the sum rule for electric dipolar transitions from the ground state (g.s.) to the states  $(n, j)$ . Using Eqs. (9) and (14) we obtain

$$S_T(E1) = \frac{3}{4\pi} \frac{Z^2 e^2 m a_{y2}}{m_2^2} (2 \cos \varphi_{23})^2 \langle \text{g.s.} | y^2 | \text{g.s.} \rangle. \quad (16)$$

If the system shows low-energy resonances coupled to the ground state by magnetic transitions at the same order than electric transitions, magnetic contributions may play a significant role. We consider then magnetic transitions, involving the matrix elements of the magnetic operator  $\widehat{M}_{\lambda M_\lambda}$ . This operator can be expressed as a sum of two terms: the orbital and spin terms [33]. Following the notation of Brink and Satchler,

$$\widehat{M}_{\lambda M_\lambda}^{\text{orb}}(\vec{r}) = \frac{e\hbar}{2mc} \sqrt{4\pi\lambda} \sum_q r_q^{\lambda-1} \frac{2g_l^{(q)}}{\lambda+1} [Y_{\lambda-1}I]_{(\lambda-1,1)\lambda, M_\lambda}^{(q)}, \quad (17)$$

$$\widehat{M}_{\lambda M_\lambda}^{\text{spin}}(\vec{r}) = \frac{e\hbar}{2mc} \sqrt{4\pi\lambda} \sum_q r_q^{\lambda-1} g_s^{(q)} [Y_{\lambda-1}S]_{(\lambda-1,1)\lambda, M_\lambda}^{(q)}. \quad (18)$$

Here  $g_l$  and  $g_s$  are the orbital and spin  $g$  factors, and  $[Y_{\lambda-1}j]_{(\lambda-1,1)\lambda, M_\lambda}$  is a tensorial product of order 1,

$$[Y_{\lambda-1}j]_{(\lambda-1,1)\lambda, M_\lambda} \equiv \sum_{\eta\nu} Y_{(\lambda-1)\eta} \sqrt{2j_\nu+1} \langle (\lambda-1)\eta 1\nu | \lambda M_\lambda \rangle. \quad (19)$$

For dipolar transitions, the total magnetic operator is given then by

$$\begin{aligned} \widehat{M}_{1M_1} &= \widehat{M}_{1M_1}^{\text{orb}} + \widehat{M}_{1M_1}^{\text{spin}} \\ &= \frac{e\hbar}{2mc} \sum_q [g_l^{(q)} I_q + g_s^{(q)} S_q]_{M_1}. \end{aligned} \quad (20)$$

These terms need to be evaluated for each particle. We express again the position of particle  $q$  in the Jacobi- $q$  system by Eq. (11), and we rotate the wave functions  $|nj\rangle$  to that system using the transformations between different Jacobi sets (see, for instance, Ref. [34]). The matrix element formula is given in Appendix A.

Transition probabilities given by Eq. (9) are a set of discrete values. In order to obtain a continuous energy distribution, the best option is to do the overlap with the continuum wave functions [35], which are not known in general. In this work, as in Ref. [24], we consider that a PS with energy  $\varepsilon_n$  is the superposition of continuum states in the vicinity. There are several ways to assign an energy distribution to a PS. Here, as in Ref. [19] we assign a Poisson distribution for each discrete value of  $B(\mathcal{O}\lambda)(\varepsilon_n)$ , with the form

$$D(\varepsilon, \varepsilon_n, w) = \frac{(w+1)^{(w+1)}}{\varepsilon_n^{w+1} \Gamma(w+1)} \varepsilon^w \exp\left(-\frac{w+1}{\varepsilon_n} \varepsilon\right), \quad (21)$$

which is properly normalized. Poisson distributions tend smoothly to zero at the origin, which is the physical behavior we expect for the energy distributions of the pseudostates. The parameter  $w$  controls the width of the distributions; as  $w$  decreases, the width of the distributions increases. The prescription to fix an appropriate  $w$  parameter will be the same as that introduced in Ref. [19]. It consists of choosing the value of  $w$  that ensures a smooth  $B(E1)$  distribution without spreading it unphysically. We present more details and a practical example in Appendix B.

### III. APPLICATION TO ${}^9\text{Be}$

The  ${}^9\text{Be}$  nucleus can be described as a three-body system, comprising two  $\alpha$  particles and one neutron. It shows a Borromean structure, since neither of the binary subsystems  ${}^5\text{He}$  nor  ${}^8\text{Be}$  are bound.  ${}^9\text{Be}$  is a loosely bound system with a  $3/2^-$  ground state located at 1.5736 MeV below the  $\alpha + \alpha + n$  threshold [36]. The presence of a very narrow two-body  ${}^8\text{Be}$  resonance at 0.092 MeV above the three-body threshold suggests a sequential description of the formation process [3]. Due to the small lifetime of the  ${}^5\text{He}$  system ( $\sim 10^{-21}$  s) compared to  ${}^8\text{Be}$  ( $\sim 10^{-16}$  s), the sequential synthesis is considered to proceed mainly through  ${}^8\text{Be}$  [37]. Nevertheless, the sequential picture may underestimate the reaction rate at low temperature by several orders of magnitude [14].

This nucleus presents a genuine three-body  $1/2^+$  resonant state around 0.11 MeV with a relatively large width [38]. Therefore, the photodissociation cross section of  ${}^9\text{Be}$  shows a relatively broad peak at the energy of the resonance, very close to the three-body and two-body thresholds. This resonance is the main contribution to the  $\alpha(\alpha n, \gamma){}^9\text{Be}$  reaction rate, especially at the lowest temperatures where other  $j^\pi$  contributions are negligible [6,14]. The experimental cross section shows also a rather narrow peak around 0.85 MeV associated with the  $5/2^-$  resonance. In this work, we have included in the calculation the  $1/2^+$ ,  $3/2^+$ ,  $5/2^+$  states, all connected to the ground state by electric dipolar ( $E1$ ) transitions. Magnetic dipolar ( $M1$ ) transitions to the  $1/2^-$ ,  $3/2^-$ ,  $5/2^-$  states are also known to have an influence on the reaction rate [3,5,6,37]. Although they are not expected to change the low-temperature tail [6], we have also calculated magnetic contributions. Our model treats the resonant and nonresonant parts of the spectrum on the same footing, both contributing to the strength function and the reaction rate.

#### A. Hamiltonian

Our three-body model includes the  $\alpha$ - $n$  potential from Ref. [39], which has been shown to provide reasonable results for  ${}^6\text{He}$  [19,24]. In order to account for the Pauli principle needed to block occupied  $\alpha$  states to the neutron, a repulsive  $s$ -wave component is introduced in the  $\alpha$ - $n$  interaction, with the requirement that the experimental phase shifts are correctly reproduced. For the  $\alpha$ - $\alpha$  nuclear interaction we include the Ali-Bodmer potential [40] version ‘‘a’’ with a different repulsive term for  $s$  and  $d$  waves:

$$V_{\alpha\alpha}(r) = (125\widehat{P}_{l=0} + 20\widehat{P}_{l=2})e^{-(r/1.53)^2} - 30e^{-(r/2.85)^2}. \quad (22)$$

In this expression, the repulsive terms block the  $\alpha$ - $\alpha$  bound states, and their strengths need to be different in order to reproduce the experimental phase shifts. This potential together with a hard-sphere Coulomb interaction with a Coulomb radius of  $r_{\text{Coul}} = 2.94$  fm,

$$V_{\alpha\alpha}^{\text{Coul}}(r) = Z^2 e^2 \times \begin{cases} \left(\frac{3}{2} - \frac{r^2}{2r_{\text{Coul}}^2}\right) \frac{1}{r_{\text{Coul}}}, & r \leq r_{\text{Coul}}, \\ \frac{1}{r}, & r > r_{\text{Coul}}, \end{cases} \quad (23)$$



TABLE I. Three-body force [Eq. (24)] parameters for different  $j^\pi$  states. See text for details on  $K_{\max}$  and  $i_{\max}$  values for each  $j^\pi$ .

$j^\pi$	$v_{3b}$ (MeV)	$r_{3b}$ (fm)	$a_{3b}$
$3/2^-$	+1.11	6.1	5
$1/2^+$	-2.45	6.1	5
$3/2^+$	-1.60	6.1	5
$5/2^+$	-0.18	6.1	5
$5/2^-$	+1.65	6.1	5
$1/2^-$	+0.20	6.1	5

reproduces the exact position of the two-body  $s$ -wave  ${}^8\text{Be}$  resonance. The modification of the Ali-Bodmer potential introduced by Fedorov *et al.* [41] should not be used in combination with the Coulomb interaction given by Eq. (23), since they do not reproduce the position of the two-body resonance, and this is crucial to obtain the right behavior in the low-lying  ${}^9\text{Be}$  continuum.

These binary interactions are adjusted to reproduce the phenomenology of the two-body systems. Since three-body models are an approximation to the full many-body system, including only two-body interactions may lead to deviations from the experimental three-body energies [15,24,34]. Therefore, it is usual to include a structureless hyperradial three-body force, which can be fixed to adjust the energy of the system without distorting its structure. We use the following expression, as in Refs. [19,24]:

$$V_{3b}(\rho) = \frac{v_{3b}}{1 + \left(\frac{\rho}{r_{3b}}\right)^{a_{3b}}}. \quad (24)$$

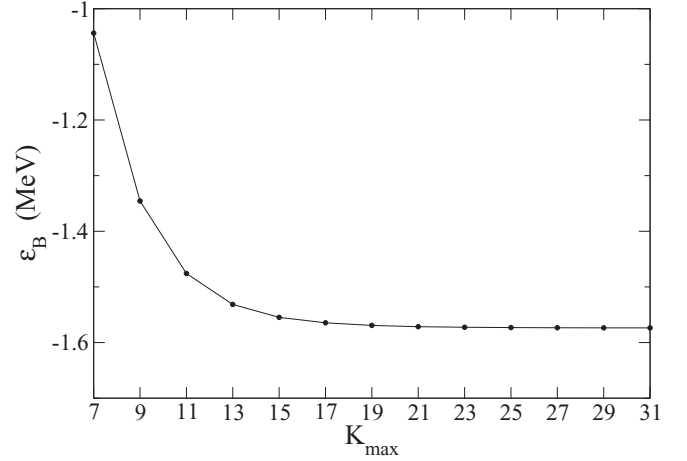
There are different choices in the literature, and we have checked that the specific form of this interaction plays a negligible role on the final results. The parameters for the three-body force are chosen to adjust the energy of the experimentally known states of the system; in this case, the ground state of  ${}^9\text{Be}$  and the  $1/2^+$ ,  $3/2^+$ ,  $5/2^+$ ,  $5/2^-$ , and  $1/2^-$  resonances. The value of these parameters are different for each  $j^\pi$  state, and they are given in Table I.

We diagonalize the Hamiltonian in a finite THO basis with a maximum value of the hypermomentum  $K_{\max}$  and a maximum number of hyperradial excitations in each channel  $i_{\max}$ . We calculate separately the kinetic energy matrix elements and the potential matrix elements. The hyperangular integration of the potential matrix elements are performed, as in Refs. [19,24], by using a set of subroutines of the code FACE [34].

### B. $3/2^-$ ground state

The  $3/2^-$  states are described with an analytical THO basis defined by parameters  $b = 0.7$  fm and  $\gamma = 1.4$  fm $^{1/2}$ , trying to minimize the size of the basis needed to reach convergence of the ground state. The three-body force parameters are taken as  $v_{3b} = 1.11$  MeV,  $r_{3b} = 6.1$  fm, and  $a_{3b} = 5$ , chosen to adjust the ground-state energy and the matter radius of  ${}^9\text{Be}$ .

In Figs. 3 and 4 we show the convergence of the ground-state energy and the matter and charge radii with respect to the maximum hypermomentum  $K_{\max}$  with  $i_{\max}$  fixed to 20.  $K_{\max}$  determines the number of channels included in the wave


 FIG. 3. Convergence of the ground-state energy of  ${}^9\text{Be}$  with respect to the maximum hypermomentum  $K_{\max}$ .

function expansion. From Fig. 3 we see that the value  $K_{\max} = 30$  provides a well converged ground state with energy  $\epsilon_B = -1.5736$  MeV in agreement with Ref. [36]. Assuming that the  $\alpha$  particle matter and charge radii are 1.47 and 1.6755 fm, respectively, for the  ${}^9\text{Be}$  ground state we obtain a charge radius of  $r_{\text{ch}} = 2.508$  fm and a matter radius of  $r_{\text{mat}} = 2.466$  fm.

Our value for the charge radius is in agreement with the experimental value of  $2.519 \pm 0.012$  fm [42]. This reveals that our description of the system is rather accurate. For the matter radius our value is larger than the one given in Ref. [43],  $2.38 \pm 0.01$  fm, obtained with Glauber-model calculations from interaction cross sections at high energies. A different estimation from a simple microscopic model by using cross sections at intermediate energies gives a radius of  $2.53 \pm 0.07$  fm [44], in better agreement with our calculation. It has been pointed out [45] that the optical limit approximation of Glauber models, such as in Ref. [43], may underestimate the radius of loosely bound systems. In halo nuclei, the few-body

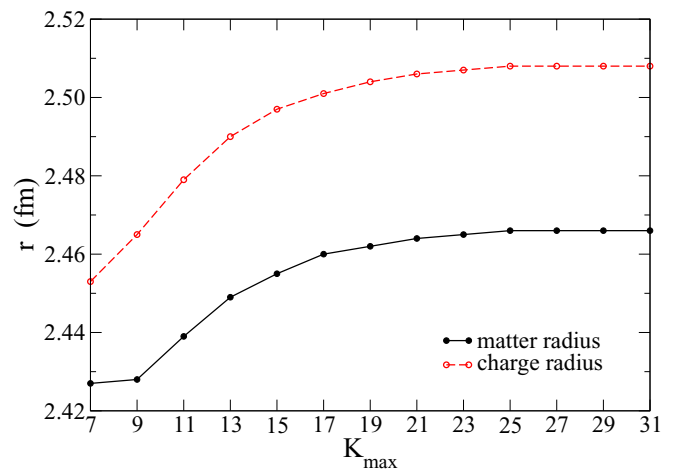

 FIG. 4. (Color online) Convergence of the matter radius (solid line) and the charge radius (dashed line) of  ${}^9\text{Be}$  with respect to the maximum hypermomentum  $K_{\max}$ .

TABLE II. Ground-state energy  $\varepsilon_B$ , matter radius  $r_{\text{mat}}$ , charge radius  $r_{\text{ch}}$ , and sum rule  $S_T(E1)$  as a function of  $i_{\text{max}}$  with  $K_{\text{max}} = 30$ . A fast convergence is observed.

$i_{\text{max}}$	$\varepsilon_B$ (MeV)	$r_{\text{mat}}$ (fm)	$r_{\text{ch}}$ (fm)	$S_T(E1)$ ( $e^2\text{fm}^2$ )
5	-1.5659	2.453	2.502	0.5565
10	-1.5734	2.465	2.507	0.5760
15	-1.5736	2.466	2.508	0.5762
20	-1.5736	2.466	2.508	0.5762
25	-1.5736	2.466	2.508	0.5762

structure implies strong spatial correlations between the core and valence nucleons, so the optical limit fails.  ${}^9\text{Be}$  is not a halo system but it shows a strong few-body intrinsic configuration with the two  $\alpha$  particles loosely bound by the remaining neutron, so the usual estimations of its radius from interaction cross sections may be misleading.

In Table II we show the convergence of the ground-state energy, its matter radius, the charge radius, and the sum rule for electric dipolar transitions [Eq. (16)] as the number of hyperradial excitations  $i_{\text{max}}$  increases. Calculations are performed for a fixed value of  $K_{\text{max}} = 30$ , and we can see a rapid convergence.

In addition, the  ${}^9\text{Be}$  system shows a large experimental quadrupole deformation, with a quadrupole moment of  $5.29 \pm 0.04$  e fm<sup>2</sup> [46]. Our model provides a good description of this deformation due to the alpha-alpha cluster configuration, and gives a quadrupole moment of 4.91 e fm<sup>2</sup>, which is close to the experimental value.

### C. $1/2^+$ resonance

The structure of the  $1/2^+$  resonance in  ${}^9\text{Be}$  has been studied by many authors, both theoretically [38,47,48] and experimentally [3,5,6,11,37], due to its relevance for the synthesis of this nucleus in astrophysics. It has been found that the radiative capture reaction  $\alpha(\alpha n, \gamma){}^9\text{Be}$  is mainly governed by the  $1/2^+$  contribution of electric dipolar transitions to the ground state [6,14].

To get a well defined  $B(E1)$  distribution at low energies, we need a basis with a large hyperradial extension to concentrate many eigenvalues close to the breakup threshold. For this purpose we describe the  $1/2^+$  states with a THO basis defined by parameters  $b = 0.7$  fm and  $\gamma = 0.7$  fm<sup>1/2</sup>.

However, our calculations show a very slow convergence with respect to  $K_{\text{max}}$  for the low-energy  $1/2^+$  continuum. The structure of the  $1/2^+$  resonance is not well described with  $K_{\text{max}}$  values around 30–40, and going to larger hypermomenta involves the computation of very large basis sets, which is limited by computer power and calculation times. Since the  $1/2^+$  resonance decay is known to proceed mainly through the two-body low-lying  $s$ -wave  ${}^8\text{Be}$  resonance [38], we expect the three-body resonance to be mainly governed by  $\alpha$ - $\alpha$   $s$ -wave components. Thus we fix  $K_{\text{max}}$  to 40 and increase the maximum hypermomentum for  $s$  waves,  $K_{\text{max}}^s$ . In Fig. 5 we show the  $1/2^+$  contribution to the total photodissociation cross section, as a function of  $K_{\text{max}}^s$ . For these calculations, we take a THO basis with  $i_{\text{max}} = 30$  and we smooth the discrete values

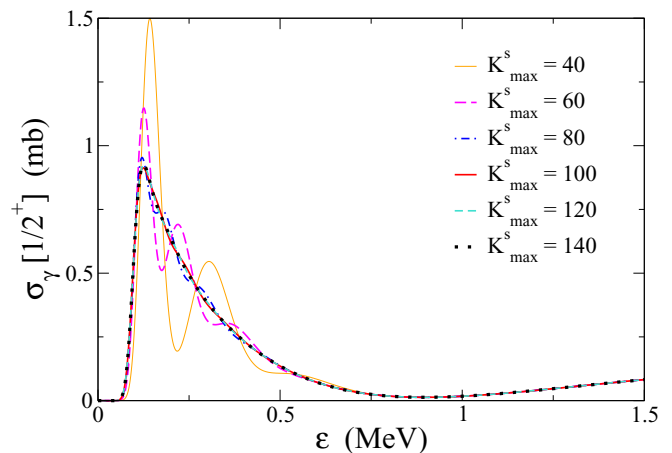


FIG. 5. (Color online) Dependence on  $K_{\text{max}}^s$  of the  $1/2^+$  contribution to the  ${}^9\text{Be}$  photodissociation cross section. (See the text.)

using Poisson distributions with a width parameter  $w = 30$ . We can see in Fig. 5 that the structure of the resonance is strongly dependent on  $K_{\text{max}}^s$ , and very large values are needed to reach convergence. For this reason, we fix  $K_{\text{max}}^s$  to 140, maintaining the global  $K_{\text{max}} = 40$  for all the other partial waves, as we find no need to include more channels in the wave function expansion to achieve converged cross section and reaction rates. The three-body-force parameters needed to reproduce the position of the resonance are  $v_{3b} = -2.45$  MeV,  $r_{3b} = 6.1$  fm, and  $a_{3b} = 5$ .

### D. $3/2^+$ , $5/2^+$ , $1/2^-$ , and $5/2^-$ states

The  $3/2^+$ ,  $5/2^+$ ,  $1/2^-$ , and  $5/2^-$  resonances in  ${}^9\text{Be}$  have excitation energies of 3.131, 1.475, 1.206, and 0.856 MeV, respectively [36]. Since these resonances contribute to the photodissociation cross section at higher energies than the case of  $1/2^+$ , we expect smaller influences on the total reaction rate, at least in the low-temperature tail. We describe these states with a THO basis defined by parameters  $b = 0.7$  fm and  $\gamma = 1.0$  fm<sup>1/2</sup>, that ensures enough states at low energies. We include all channels up to  $K_{\text{max}} = 30$ , large enough to get converged strength distributions in these cases, and  $i_{\text{max}} = 30$ . In order to adjust the position of the resonances, we change the parameter  $v_{3b}$  to  $-1.60$  MeV for the  $3/2^+$  states,  $-0.18$  MeV for the  $5/2^+$ ,  $+1.65$  MeV for the  $5/2^-$  states, and  $+0.20$  for the  $1/2^-$  states. The  $B(E1)$  and  $B(M1)$  discrete values are smoothed using Poisson distributions with a width parameter  $w = 30, 60, 30$  for  $3/2^+, 5/2^+, 1/2^-$ , respectively. For the  $5/2^-$  states we need a larger width parameter, which produces narrower distributions, since the  $5/2^-$  resonance shows a very small width. This was previously reported in Ref. [24], where a value of  $w = 1300$  was used to describe properly the width of the narrow  $2^+$  resonance in  ${}^6\text{He}$ . Thus we fix  $w = 10000$  around the resonance energy for the  $5/2^-$  states, keeping  $w = 30$  for the nonresonant region.

Note that the convergence problem shown in the preceding subsection for the  $1/2^+$  state is absent in these cases. These resonances have larger excitation energies, and thus their properties are less sensitive to the  $\alpha$ - $\alpha$   $s$ -wave contribution.

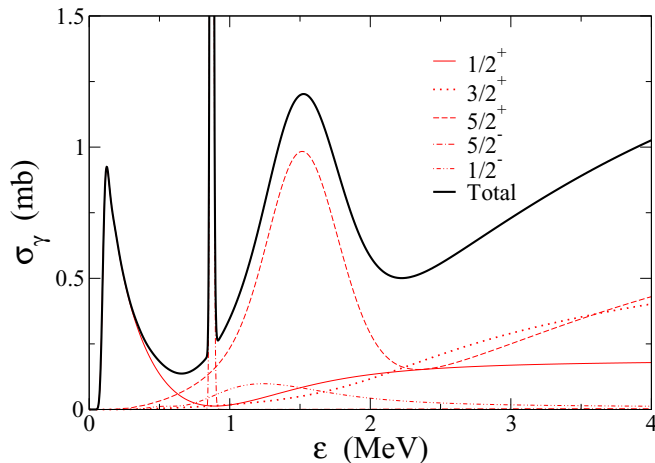


FIG. 6. (Color online) Contribution of the  $1/2^+$  (thin solid),  $5/2^+$  (dashed),  $3/2^+$  (dotted),  $5/2^-$  (dot dashed), and  $1/2^-$  (double dot dashed) states to the total photodissociation cross section (thick solid).

### E. Photodissociation cross section

In Fig. 6, we show the three electric dipolar contributions to the photodissociation cross section of  ${}^9\text{Be}$  from  $1/2^+$  (thin full line),  $3/2^+$  (dotted line), and  $5/2^+$  (dashed line) states. We include also the magnetic dipolar contribution from the  $5/2^-$  states (dot dashed) and the  $1/2^-$  states (double dot dashed). The total cross section is also shown by a thick full line. We can see how at very low energy only the  $1/2^+$  states contribute to the cross section.

In Fig. 7, we compare the result shown in Fig. 6 with the experimental data from Arnold *et al.* [6] and Sumiyoshi *et al.* [3]. The agreement is rather good. Although we do not include them in the figure for clarity, our results are also in good agreement with other experimental data available in the literature [5,37]. We show also recent calculations by de Diego *et al.* [15,49] using a similar three-body model. In these works,

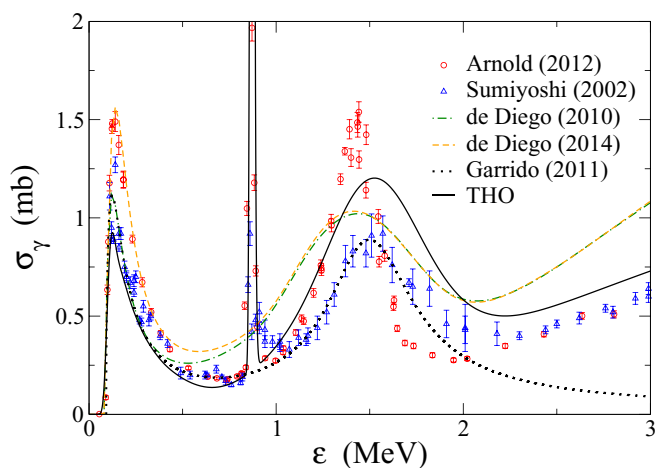


FIG. 7. (Color online) Total photodissociation from our three-body calculation (solid line) compared with the results from Refs. [49] (dashed line), [15] (dot dashed), and [14] (dotted) and experimental data of Refs. [3] (triangles) and [6] (circles).

the continuum problem is solved by imposing box boundary conditions, for which obtaining a large density of states at the lowest energies is numerically challenging. So, the  $1/2^+$  resonance peak for energies below 1.2 MeV is replaced by an energy-dependent Breit-Wigner distribution with the proper resonance parameters to reproduce the data. In Ref. [15], the  $1/2^+$  parameters are adjusted to reproduce the 2002 data, while those in Ref. [49] are fixed to describe the 2012 data. This procedure is applied by Garrido *et al.* [14] to fit the total cross section including Breit-Wigner distributions for the lowest  ${}^9\text{Be}$  resonances, and we also include this result in Fig. 7. This calculation is adjusted to reproduce the data from Sumiyoshi *et al.*

In contrast, our calculated  $1/2^+$  peak is directly obtained by smoothing the transition strength following Eq. (21), using a THO basis that concentrates a large density of states near the breakup threshold. In this sense, our model provides the first full three-body calculation of the  ${}^9\text{Be}$  photodissociation cross section in the whole energy range. We underestimate the experimental data for the  $1/2^+$  contribution (in particular compared to 2012 data), but it shows the right low-energy behavior and the corresponding tail of the resonance. The smaller height is not crucial when computing the reaction rate, an observable that ranges over many orders of magnitude as a function of the temperature, especially at the lowest temperatures where the rate is strongly governed by the cross section behavior up to 0.1–0.2 MeV only.

We reproduce very well the narrow  $5/2^-$  resonance, although we know from sequential models that this contribution has a small influence on the total reaction rate [5,6]. This contribution is not computed in Refs. [14,15,49]. Concerning the  $5/2^+$  broad resonance, our three-body estimations agree better with Sumiyoshi *et al.* [3] than with those from the more recent experiment of Arnold *et al.* [6], in which a rather narrow peak is obtained. For that reason we fix the position of the  $5/2^+$  resonance to Sumiyoshi *et al.* data. In the calculations by de Diego *et al.*, the  $5/2^+$  resonance is adjusted to the energy given by Sumiyoshi *et al.*; however, due to the smoothing procedure the maximum is shifted to lower energy.

The  $3/2^+$  resonance plays a minor role and its contribution affects only the high energy region. At these energies, our calculations agree better with both sets of experimental data than those by de Diego *et al.* The overall difference between both calculations could be associated with the different discretization methods and different two-body potentials. We have also estimated the  $M1$  contribution to the  $1/2^-$  states, which has a small effect on the cross section, as shown in Fig. 6.

As we can see in Fig. 7, although the overall behavior is very similar in both sets of experimental data, there are important discrepancies between them. The accuracy of these experiments could then be questioned, since experimental normalization factors may lead to very different results. In Refs. [3,6], for instance, the energy and width of the  $1/2^+$  resonance are found to be the same, but with gamma widths differing by a factor of 1.3. This results in a different height for the resonant peak. For that reason it is not trivial to find an explanation of the differences between theory and experiment. We must also consider that three-body models

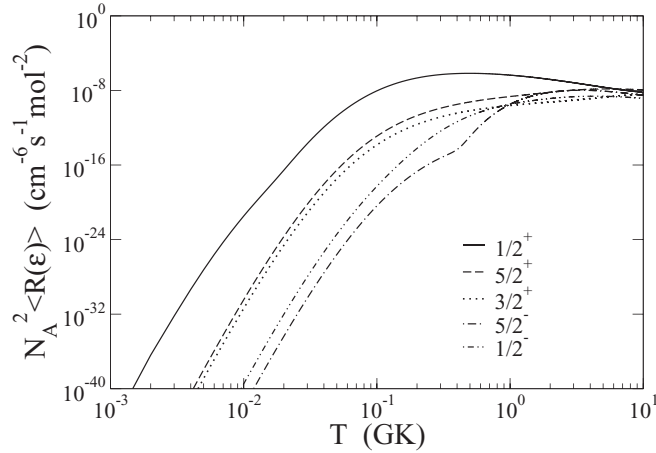


FIG. 8. Contribution of the  $1/2^+$  (thin solid),  $5/2^+$  (dashed),  $3/2^+$  (dotted),  $5/2^-$  (dot dashed), and  $1/2^-$  (double dot dashed) states to the total reaction rate.

are an approximation to the actual many-body problem, and consequently there might be effects on the cross section that we are not considering explicitly, e.g., dynamical effects within the clusters, full antisymmetrization problems, etc. Both calculations (this work and Refs. [15,49]) are systematically above the data at energies larger than 2 MeV, but at this level it is not possible to determine if this difference is related to many-body corrections or a possible normalization uncertainty. In any case, the final reaction rate at low temperature depends mainly on the photodissociation cross section at the lowest energies (0–0.2 MeV) and the total strength, so differences in the height, shape, etc. of the specific structures are not crucial.

### F. Reaction rate

We compute the rate of the radiative capture reaction  $\alpha + n \rightarrow {}^9\text{Be} + \gamma$  from the photodissociation cross section, according to Eq. (7). In Fig. 8 we show the contributions from the  $1/2^+$  (solid line),  $3/2^+$  (dotted line),  $5/2^+$  (dashed line),  $5/2^-$  (dot dashed), and  $1/2^-$  (double dot dashed) states to the reaction rate. We can see that the  $1/2^+$  states dominates over all other contributions, especially in the low-temperature tail of the reaction rate. The other contributions become relevant at temperatures above 3 GK.

In Table III we present the total reaction rate, the sum of the electric and magnetic dipolar contributions, at representative temperatures. In Fig. 9 we compare this rate with sequential estimations from experimental cross sections [3,6,11]. Our three-body model converges to the sequential result at high temperature, where the direct capture plays a minor role. Calculations by de Diego *et al.* [15,49] between 0.1 and 5 GK also agree with this results, although we do not include them in Fig. 9 for clarity. At low temperature, below 0.1 GK, the three-body capture enhances the reaction rate in several orders of magnitude, in good agreement with three-body Breit-Wigner estimations by Garrido *et al.* [14]. This confirms that the uncertainty related to the  $1/2^+$  resonance peak is not crucial when computing the reaction rate, as discussed in Sec. III E. At such low temperatures the three-body system

TABLE III. Reaction rate of  $\alpha n$ , in  $\text{cm}^{-6}\text{s}^{-1}\text{mol}^{-2}$ , at representative temperatures in GK,  $T_9$ .

$T_9$	Rate	$T_9$	Rate	$T_9$	Rate
0.001	$3.67 \times 10^{-45}$	0.04	$1.16 \times 10^{-12}$	0.45	$6.78 \times 10^{-7}$
0.002	$4.03 \times 10^{-37}$	0.05	$1.83 \times 10^{-11}$	0.5	$6.85 \times 10^{-7}$
0.003	$6.19 \times 10^{-33}$	0.06	$1.31 \times 10^{-10}$	0.6	$6.61 \times 10^{-7}$
0.004	$4.57 \times 10^{-30}$	0.07	$5.71 \times 10^{-10}$	0.7	$6.10 \times 10^{-7}$
0.005	$5.75 \times 10^{-28}$	0.08	$1.78 \times 10^{-9}$	0.8	$5.52 \times 10^{-7}$
0.006	$2.48 \times 10^{-26}$	0.09	$4.38 \times 10^{-9}$	0.9	$4.94 \times 10^{-7}$
0.007	$5.17 \times 10^{-25}$	0.1	$9.07 \times 10^{-9}$	1	$4.41 \times 10^{-7}$
0.008	$6.41 \times 10^{-24}$	0.11	$1.65 \times 10^{-8}$	1.25	$3.32 \times 10^{-7}$
0.009	$5.41 \times 10^{-23}$	0.12	$2.71 \times 10^{-8}$	1.5	$2.53 \times 10^{-7}$
0.011	$3.40 \times 10^{-22}$	0.13	$4.11 \times 10^{-8}$	1.75	$1.98 \times 10^{-7}$
0.012	$7.15 \times 10^{-21}$	0.14	$5.85 \times 10^{-8}$	2	$1.58 \times 10^{-7}$
0.013	$2.61 \times 10^{-20}$	0.15	$7.93 \times 10^{-8}$	2.5	$1.07 \times 10^{-7}$
0.014	$8.55 \times 10^{-20}$	0.16	$1.03 \times 10^{-7}$	3	$7.89 \times 10^{-8}$
0.015	$2.57 \times 10^{-19}$	0.17	$1.29 \times 10^{-7}$	3.5	$6.18 \times 10^{-8}$
0.016	$7.25 \times 10^{-19}$	0.18	$1.57 \times 10^{-7}$	4	$5.09 \times 10^{-8}$
0.017	$1.93 \times 10^{-18}$	0.19	$1.87 \times 10^{-7}$	5	$3.85 \times 10^{-8}$
0.018	$4.91 \times 10^{-18}$	0.2	$2.18 \times 10^{-7}$	6	$3.19 \times 10^{-8}$
0.019	$1.19 \times 10^{-17}$	0.25	$3.72 \times 10^{-7}$	7	$2.79 \times 10^{-8}$
0.02	$2.79 \times 10^{-17}$	0.3	$5.01 \times 10^{-7}$	8	$2.52 \times 10^{-8}$
0.025	$1.11 \times 10^{-15}$	0.35	$5.93 \times 10^{-7}$	9	$2.34 \times 10^{-8}$
0.03	$1.95 \times 10^{-14}$	0.4	$6.49 \times 10^{-7}$	10	$2.20 \times 10^{-8}$

has no energy to populate the two-body  ${}^8\text{Be}$  resonance and, as expected, the direct capture begins to dominate. This effect cannot be described with sequential models.

## IV. SUMMARY AND CONCLUSIONS

The structure of the Borromean nucleus  ${}^9\text{Be}$  ( $\alpha + \alpha + n$ ) has been described in a full three-body model using the analytical THO method. The photodissociation cross section is calculated including electric dipolar transitions from the  $3/2^-$  ground state to the  $1/2^+$ ,  $3/2^+$ ,  $5/2^+$  continuum states

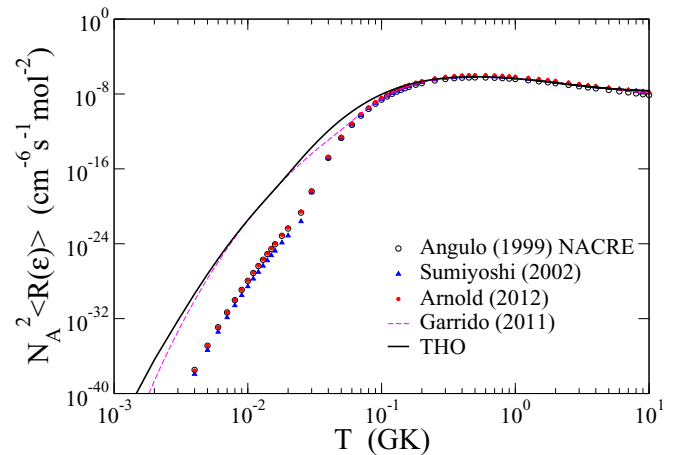


FIG. 9. (Color online) Total reaction rate from our three-body calculation (solid line) and three-body Breit-Wigner calculation [14] (dashed line) compared with sequential estimations from experimental data of Refs. [11] (squares), [3] (triangles), and [6] (circles).



and also magnetic transitions to the  $5/2^-$  and  $1/2^-$  states. For each angular momentum, an appropriate analytical THO basis has been used. The results show the dominance of the  $1/2^+$  resonance at low energy. The comparison with the experimental data and with previous calculations available in the literature reveals the effectiveness of the formalism.

The difference between theoretical works is discussed. Unlike previous calculations, our model describes the photodissociation cross section using the same footing in the whole energy range. The differences between theory and experiments might be related to many-body corrections not included within three-body models and also to experimental uncertainties arising from the discrepancies between the different data sets.

The radiative capture reaction rate for the formation of  ${}^9\text{Be}$  is then calculated from the photodissociation cross section. The reaction rate so obtained within a full three-body model matches the reaction rates obtained using sequential models at temperatures above 0.1 GK. However at lower temperatures the three-body calculation is several orders of magnitude larger than the sequential models. This result reveals that the sequential models fail to reproduce the capture reaction rate of  ${}^9\text{Be}$  at low temperature where the three-body system has no energy to populate the two-body  ${}^8\text{Be}$  resonance and the direct capture becomes more relevant. Our calculations agree reasonably well with estimations using three-body Breit-Wigner distributions to fit the cross section.

The successful application of the analytical THO method to the determination of the  ${}^9\text{Be}$  photodissociation cross section and radiative capture reaction rate encourages the application to the triple-alpha process as well as the formation of  ${}^{17}\text{Ne}$  ( ${}^{15}\text{O} + p + p$ ). Both reactions involve three charged particles, which increases the level of difficulty.

### ACKNOWLEDGMENTS

Authors are grateful to P. Descouvemont, E. Garrido, and J. Gómez-Camacho for useful discussions and suggestions. This work has been partially supported by the Spanish Ministerio de Economía y Competitividad under Projects FPA2009-07653 and FIS2011-28738-c02-01, by Junta de Andalucía under group number FQM-160 and Project P11-FQM-7632, and by the Consolider-Ingenio 2010 Programme CPAN (CSD2007-00042). This work was performed under the auspices of the US Department of Energy by Lawrence Livermore National Laboratory under Contract DE-AC52-07NA27344. J. Casal acknowledges a FPU research grant from the Ministerio de Educación, Cultura y Deporte, AP2010-3124.

### APPENDIX A: MAGNETIC OPERATOR MATRIX ELEMENTS

In this Appendix, we present the main expressions needed to compute the magnetic operator matrix elements from Eq. (18). For each particle  $q$ , we rotate the wave function given by Eq. (6) to the Jacobi- $q$  system, and then we sum up the orbital and spin contributions. This can be expressed in a compact form by using the transformations between different Jacobi sets for

the angular part of the wave functions [34],

$$N_{\beta_k\beta_q} = \langle k : \beta_k j \mu | q : \beta_q j \mu \rangle. \quad (\text{A1})$$

Here index  $q$  labels particle  $q$ , while  $k$  denotes the preferred Jacobi system in which we diagonalize the Hamiltonian. Since  $k$  is fixed, we omit it for the following expressions, so  $|k : \beta_k j \mu\rangle$  represents  $\mathcal{Y}_{\beta_j \mu}(\Omega)$  in Eq. (3). These functions are expanded in hyperspherical harmonics (HH) [25,26]  $\Upsilon_{K l m_l}^{l_x l_y}(\Omega)$  as

$$\mathcal{Y}_{\beta_j \mu}(\Omega) = \sum_{\nu l} \langle j_{ab} \nu l | j \mu \rangle \kappa_l^{\nu} \sum_{m_l \sigma} \langle l m_l S_x \sigma | j_{ab} \nu \rangle \Upsilon_{K l m_l}^{l_x l_y}(\Omega) \chi_{S_x}^{\sigma}. \quad (\text{A2})$$

Here  $\chi_{S_x}^{\sigma}$  is the spin wave function of the two particles related by the Jacobi coordinate  $\mathbf{x}$  and  $\kappa_l^{\nu}$  is the spin function of the third particle. The HH are eigenfunctions of the hypermomentum operator  $\widehat{K}^2$ , and can be expressed in terms of the spherical harmonics as

$$\Upsilon_{K l m_l}^{l_x l_y}(\Omega) = \sum_{m_x m_y} \langle l_x m_x l_y m_y | l m_l \rangle \Upsilon_K^{l_x l_y m_x m_y}(\Omega), \quad (\text{A3})$$

$$\Upsilon_K^{l_x l_y m_x m_y}(\Omega) = \varphi_K^{l_x l_y}(\alpha) Y_{l_x m_x}(\widehat{\mathbf{x}}) Y_{l_y m_y}(\widehat{\mathbf{y}}), \quad (\text{A4})$$

$$\varphi_K^{l_x l_y}(\alpha) = N_K^{l_x l_y} (\sin \alpha)^{l_x} (\cos \alpha)^{l_y} P_n^{l_x + \frac{1}{2}, l_y + \frac{1}{2}}(\cos 2\alpha), \quad (\text{A5})$$

where  $P_n^{a,b}$  is a Jacobi polynomial with order  $n = (K - l_x - l_y)/2$  and  $N_K^{l_x l_y}$  is the normalization constant.

Using Eq. (A1) and expanding the explicit angular dependence of the wave functions, we can express the orbital and spin parts of the magnetic operator reduced matrix element for

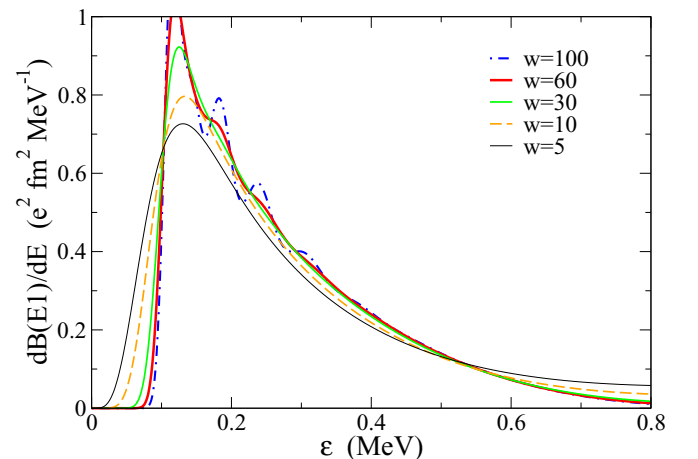


FIG. 10. (Color online)  $B(E1)$  distribution to the  $1/2^+$  states as a function of the Poisson width parameter  $w$ . (See text for details.)

a given multipolarity  $\lambda$  as

$$\begin{aligned} \langle nj || \widehat{M}_\lambda^{\text{orb}} || n' j' \rangle &= \frac{e\hbar}{2mc} \frac{\sqrt{\lambda}}{\lambda + 1} (\lambda - 1) \hat{\lambda} \hat{j}' (-1)^\lambda \sum_q \left( \frac{M_T - m_q}{M_T} \right)^\lambda \left( \frac{m}{a_{y_q}} \right)^{\frac{\lambda-1}{2}} 2g_l^{(q)} \sum_{\beta\beta'} \sum_{\beta_q\beta'_q} N_{\beta\beta_q} N_{\beta\beta'_q} \delta_{S_{x_q} S'_{x_q}} \delta_{l_{x_q} l'_{x_q}} \\ &\times (-1)^{2j-j'+l'_{y_q}-l_{y_q}+l_{x_q}-S_{x_q}+j_{ab_q}+j'_{ab_q}-l_q} \sqrt{l'_{y_q}(l'_{y_q}+1)} \hat{l}_{y_q} \hat{l}_{y_q}^2 \hat{j}_{ab_q} \hat{j}'_{ab_q} \hat{l}_q \hat{l}'_q \begin{pmatrix} l_{y_q} & \lambda-1 & l'_{y_q} \\ 0 & 0 & 0 \end{pmatrix} \\ &\times W(l_{y_q} l'_{y_q} (\lambda-1) 1; \lambda l'_{y_q}) W(l_q l'_q l_{y_q} l'_{y_q}; \lambda l_{x_q}) W(l_{y_q} l'_{y_q} (\lambda-1) 1; \lambda l'_{y_q}) W(l_{y_q} l'_{y_q} (\lambda-1) 1; \lambda l'_{y_q}) \\ &\times \sum_{ii'} C_n^{i\beta j} C_n^{i'\beta' j'} \iint d\alpha d\rho (\sin \alpha)^2 (\cos \alpha)^2 U_{i\beta}(\rho) \varphi_{K_q}^{l_{x_q} l_{y_q}}(\alpha) y^{\lambda-1} U_{i'\beta'}(\rho) \varphi_{K'_q}^{l'_{x_q} l'_{y_q}}(\alpha), \end{aligned} \quad (\text{A6})$$

$$\begin{aligned} \langle nj || \widehat{M}_\lambda^{\text{spin}} || n' j' \rangle &= \frac{e\hbar}{2mc} \sqrt{\lambda} (\lambda - 1) \hat{\lambda} \hat{j}' \sum_q \left( \frac{M_T - m_q}{M_T} \right)^{\lambda-1} \left( \frac{m}{a_{y_q}} \right)^{\frac{\lambda-1}{2}} g_s^{(q)} \sum_{\beta\beta'} \sum_{\beta_q\beta'_q} N_{\beta\beta_q} N_{\beta\beta'_q} \delta_{S_{x_q} S'_{x_q}} \delta_{l_{x_q} l'_{x_q}} \\ &\times (-1)^{j+j'+l_{x_q}-S_{x_q}-j_{ab_q}+2l_q} \sqrt{l_q(l_q+1)} \hat{l}_q \hat{l}_{y_q} \hat{l}'_{y_q} \hat{j}_{ab_q} \hat{j}'_{ab_q} \hat{l}_q \hat{l}'_q \begin{pmatrix} l_{y_q} & \lambda-1 & l'_{y_q} \\ 0 & 0 & 0 \end{pmatrix} \\ &\times W(l_q l'_q l_{y_q} l'_{y_q}; (\lambda-1) l_{x_q}) W(l_q l'_q j_{ab_q} j'_{ab_q}; (\lambda-1) S_{x_q}) \begin{Bmatrix} j & j' & \lambda \\ j_{ab_q} & j'_{ab_q} & \lambda-1 \\ I_q & I_q & 1 \end{Bmatrix} \\ &\times \sum_{ii'} C_n^{i\beta j} C_n^{i'\beta' j'} \iint d\alpha d\rho (\sin \alpha)^2 (\cos \alpha)^2 U_{i\beta}(\rho) \varphi_{K_q}^{l_{x_q} l_{y_q}}(\alpha) y^{\lambda-1} U_{i'\beta'}(\rho) \varphi_{K'_q}^{l'_{x_q} l'_{y_q}}(\alpha). \end{aligned} \quad (\text{A7})$$

The notation  $\hat{j}$  represents a reduced form for the factor  $\sqrt{2j+1}$ . These expressions depend on the orbital and spin  $g$  factors of each particle. The  $\alpha$  particles have spin zero, so we consider  $g_s^{(\alpha)} = 0$  and  $g_l^{(\alpha)}$  is taken as its charge. For the neutron we use the free value of  $g_s^{(n)} = -3.82$  and we do not assign any effective charge, so  $g_l^{(n)} = 0$ . It is known that the effective  $g$  factors are rather uncertain [50], especially  $g_s^{(n)}$  which could be reduced by a factor of 2 due to spin polarization. A more exhaustive analysis of these factors for the particular case of  ${}^9\text{Be}$  could reduce the uncertainty in the magnetic contributions to the photodissociation cross section.

## APPENDIX B: SMOOTHING PROCEDURE

In PS methods any transition probability to be calculated is given by a set of discrete values. In order to obtain a continuous

distribution, in this work we assign a Poisson distributions to each PS. We discuss in this Appendix the procedure to select an optimal width parameter  $w$  for the Poisson distributions defined by Eq. (21). The value of  $w$  must ensure a smooth  $B(E1)$  distribution without spreading it unphysically. As an example, we show in Fig. 10 the  $B(E1)$  distribution to the  $1/2^+$  states calculated with different width parameters. For  $w$  values smaller than 30, the distributions are too wide to represent the PS energy distributions, and consequently the final distributions cannot reproduce the experimental photodissociation data. For much larger values, however, the final distributions are distorted and show unphysical oscillations or peaks. This is our prescription to select the optimal  $w$  value; that is,  $w$  as large as possible. In this case  $w = 30$  is a reasonable choice. This method provides good results and a rather good agreement with the experimental data on the photodissociation cross section, as shown in Sec. III E.

- [1] F. Hoyle, *Astrophys. J. Suppl. Ser.* **1**, 121 (1954).
- [2] A. Aprahamian, K. Langanke, and M. Wiescher, *Prog. Part. Nucl. Phys.* **54**, 535 (2005).
- [3] K. Sumiyoshi, H. Utsunomiya, S. Goko, and T. Kajino, *Nucl. Phys. A* **709**, 467 (2002).
- [4] V. D. Efros, H. Oberhummer, A. Pushkin, and I. J. Thompson, *Eur. Phys. J. A* **1**, 447 (1998).
- [5] O. Burda, P. von Neumann-Cosel, A. Richter, C. Forssén, and B. A. Brown, *Phys. Rev. C* **82**, 015808 (2010).
- [6] C. W. Arnold, T. B. Clegg, C. Iliadis, H. J. Karwowski, G. C. Rich, J. R. Tompkins, and C. R. Howell, *Phys. Rev. C* **85**, 044605 (2012).

- [7] A. Mengoni and T. Otsuka, in *10th International Symposium on Capture Gamma-Ray Spectroscopy and Related Topics, 1999, Sante Fe*, edited by S. Wender, AIP Conf. Proc. No. 529 (AIP, New York, 2000), p. 119.
- [8] T. Sasaki, K. T. Kajino, G. Mathews, K. Otsuki, and T. Nakamura, *Astrophys. J.* **634**, 1173 (2005).
- [9] V. D. Efros, W. Balogh, H. Herndl, R. Hofinger, and H. Oberhummer, *Z. Phys. A* **355**, 101 (1996).
- [10] W. A. Fowler, G. R. Caughlan, and B. A. Zimmerman, *Annu. Rev. Astron. Astrophys.* **5**, 525 (1967).
- [11] C. Angulo *et al.*, *Nucl. Phys. A* **656**, 3 (1999).

- [12] L. V. Grigorenko, K. Langanke, N. B. Shulgina, and M. V. Zhukov, *Phys. Lett. B* **641**, 254 (2006).
- [13] R. Álvarez-Rodríguez, H. O. U. Fynbo, A. S. Jensen, and E. Garrido, *Phys. Rev. Lett.* **100**, 192501 (2008).
- [14] E. Garrido, R. de Diego, D. V. Fedorov, and A. S. Jensen, *Eur. Phys. J. A* **47**, 102 (2011).
- [15] R. de Diego, E. Garrido, D. V. Fedorov, and A. S. Jensen, *Eur. Phys. Lett.* **90**, 52001 (2010).
- [16] N. B. Nguyen, F. M. Nunes, I. J. Thompson, and E. F. Brown, *Phys. Rev. Lett.* **109**, 141101 (2012).
- [17] N. B. Nguyen, F. M. Nunes, and I. J. Thompson, *Phys. Rev. C* **87**, 054615 (2013).
- [18] S. Ishikawa, *Phys. Rev. C* **87**, 055804 (2013).
- [19] J. Casal, M. Rodríguez-Gallardo, and J. M. Arias, *Phys. Rev. C* **88**, 014327 (2013).
- [20] J. Casal, M. Rodríguez-Gallardo, and J. M. Arias, in *La Rabida 2012 International Scientific Meeting on Nuclear Physics: Basic Concepts in Nuclear Physics: Theory, Experiments, and Applications, 2013, La Rábida, Spain*, edited by J. A. Caballero Carretero, C. E. Alonso Alonso, M. V. Andrés Martín, J. E. Garcia Ramos, and F. Pérez Bernal, AIP Conf. Proc. No. 1541 (AIP, New York, 2013), p. 171.
- [21] J. A. Lay, A. M. Moro, J. M. Arias, and J. Gómez-Camacho, *Phys. Rev. C* **82**, 024605 (2010).
- [22] A. M. Moro, J. M. Arias, J. Gómez-Camacho, and F. Pérez-Bernal, *Phys. Rev. C* **80**, 054605 (2009).
- [23] R. Álvarez-Rodríguez, A. S. Jensen, D. V. Fedorov, H. O. U. Fynbo, and E. Garrido, *Phys. Rev. Lett.* **99**, 072503 (2007).
- [24] M. Rodríguez-Gallardo, J. M. Arias, J. Gómez-Camacho, A. M. Moro, I. J. Thompson, and J. A. Tostevin, *Phys. Rev. C* **72**, 024007 (2005).
- [25] M. V. Zhukov, B. V. Danilin, D. V. Fedorov, J. M. Bang, I. J. Thompson, and J. S. Vaagen, *Phys. Rep.* **231**, 151 (1993).
- [26] M. Rodríguez-Gallardo, Ph.D. thesis, Universidad de Sevilla, 2005.
- [27] S. Karataglidis, K. Amos, and B. G. Giraud, *Phys. Rev. C* **71**, 064601 (2005).
- [28] C. Forssén, N. B. Shul'gina, and M. V. Zhukov, *Phys. Rev. C* **67**, 045801 (2003).
- [29] J. M. Blatt and V. F. Weisskopf, *Theoretical Nuclear Physics* (John Wiley and Sons, New York, 1966).
- [30] D. M. Brink and G. R. Satchler, *Angular Momentum* (Clarendon, Oxford, 1994).
- [31] E. Nielsen, D. V. Fedorov, A. S. Jensen, and E. Garrido, *Phys. Rep.* **347**, 373 (2001).
- [32] R. de Diego, E. Garrido, A. S. Jensen, and D. V. Fedorov, *Phys. Rev. C* **77**, 024001 (2008).
- [33] A. Bohr and B. R. Mottelson, *Nuclear Structure* (W. A. Benjamin, Inc., Reading, MA, 1969).
- [34] I. J. Thompson, F. M. Nunes, and B. V. Danilin, *Comput. Phys. Commun.* **161**, 87 (2004).
- [35] M. Rodríguez-Gallardo and A. M. Moro, *Int. J. Mod. Phys. E* **20**, 947 (2011).
- [36] D. R. Tilley, J. H. Kelley, J. L. Godwin, D. J. Millener, J. E. Purcell, C. G. Sheu, and H. R. Weller, *Nucl. Phys. A* **745**, 155 (2004).
- [37] H. Utsunomiya, Y. Yonezawa, H. Akimune, T. Yamagata, M. Ohta, M. Fujishiro, H. Toyokawa, and H. Ohgaki, *Phys. Rev. C* **63**, 018801 (2000).
- [38] E. Garrido, D. V. Fedorov, and A. S. Jensen, *Phys. Lett. B* **684**, 132 (2010).
- [39] I. J. Thompson, B. V. Danilin, V. D. Efros, J. S. Vaagen, J. M. Bang, and M. V. Zhukov, *Phys. Rev. C* **61**, 024318 (2000).
- [40] S. Ali and A. R. Bodmer, *Nucl. Phys.* **80**, 99 (1966).
- [41] D. V. Fedorov, A. S. Jensen, and K. Riisager, *Phys. Lett. B* **312**, 1 (1993).
- [42] I. Angeli and K. P. Marinova, *At. Data Nucl. Data Tables* **99**, 69 (2013).
- [43] I. Tanihata *et al.*, *Phys. Lett. B* **206**, 592 (1988).
- [44] E. Liatard *et al.*, *Europhys. Lett.* **13**, 401 (1990).
- [45] J. S. Al-Khalili and J. A. Tostevin, *Phys. Rev. Lett.* **76**, 3903 (1996).
- [46] D. Sundholm and J. Olsen, *Chem. Phys. Lett.* **177**, 91 (1991).
- [47] V. D. Efros and J. M. Bang, *Eur. Phys. J. A* **4**, 33 (1999).
- [48] J. Görres, H. Herndl, I. J. Thompson, and M. Wiescher, *Phys. Rev. C* **52**, 2231 (1995).
- [49] R. de Diego, E. Garrido, D. V. Fedorov, and A. S. Jensen, *Eur. Phys. J. A* **50**, 93 (2014).
- [50] C. Romero-Redondo, E. Garrido, D. V. Fedorov, and A. S. Jensen, *Phys. Rev. C* **77**, 054313 (2008).